University of Groningen

Unravelling Light-Induced Degradation of Layered Perovskite Crystals and Design of Efficient Encapsulation for Improved Photostability

Fang, Hong-Hua; Yang, Jie; Tao, Shuxia; Adjokatse, Sampson; Kamminga, Machteld; Ye, Jianting; Blake, Graeme; Even, Jacky; Loi, Maria

IMPORTANT NOTE: You are advised to consult the publisher's version (publisher's PDF) if you wish to cite from it. Please check the document version below.

Document Version
Publisher's PDF, also known as Version of record

Publication date:
2018

Link to publication in University of Groningen/UMCG research database

FULL PAPER

Layered Perovskite

ADVANCED
FUNCTIONAL
MATERIALS

www.afm-journal.de

Unravelling Light-Induced Degradation of Layered Perovskite Crystals and Design of Efficient Encapsulation for Improved Photostability

Hong-Hua Fang, Jie Yang,* Shuxia Tao, Sampson Adjokatse, Machteld E. Kamminga, Jianting Ye, Graeme R. Blake, Jacky Even, and Maria Antonietta Loi*

Layered halide perovskites have recently shown extraordinary potential for low-cost solution-processable optoelectronic applications because of their superior moisture stability over their 3D counterparts. However, few studies have investigated the effect of light on layered hybrid perovskites. Here, the mechanically exfoliated nanoflakes of the 2D perovskite $(PEA)_2PbI_4$ (PEA, 2-phenylethylammonium) are used as a model to investigate their intrinsic photostability. The light-induced degradation of the flakes is investigated by using in situ techniques including confocal laser scanning microscopy, wide-field fluorescence microscopy, and atomic force microscopy. Under resonant photoexcitation, $(PEA)_2PbI_4$ degrades to PbI_2. It is clearly shown that this process is initiated at the crystal edges and from the surface. As a consequence, the photoluminescence of $(PEA)_2PbI_4$ is progressively quenched by surface traps. Importantly, the light-induced degradation can be suppressed by encapsulation using hexagonal boron nitride (hBN) flakes and/or polycarbonates. This report sheds light on a specific mechanism of light-induced degradation in layered perovskites and proposes a new encapsulation method to improve their photostability.

1. Introduction

Hybrid organic–inorganic metal halide perovskites (such as $CH_3NH_3PbX_3$, X = Cl, Br, I) have shown great promise for high performance and low-cost photovoltaics.[1–3] Despite their impressive power conversion efficiency, these perovskites suffer from decomposition under ambient conditions.[4–6] Stability issues are among the most important obstacles to large-scale commercial applications of halide perovskites, in solar cells and other optoelectronic devices. Recently, phase-pure Ruddlesden–Popper multilayered perovskites (RPPs) have been introduced in perovskite solar cells and light-emitting devices to improve both their photostability and moisture resistance.[7–9] Using 2D/3D perovskite mixtures, solar modules have been shown to be stable for more than 10 000 h.[10] In addition to moisture, light and oxygen constitute stressors which play key roles in the instability of perovskite devices.[5,11,12]

Earlier work on 3D perovskites showed that light can either heal or break down the perovskite lattice.[12–15] For instance, deQuilettes et al. observed photoinduced halide migration with strongly correlated photoluminescence (PL) intensity.[16] Yuan et al. reported light-induced degradation in $CH_3NH_3PbI_3$ films, which break down into a scattered distribution of submicron particles.[17] Merdasa et al. also found a PL intensity decrease and a blue-shift of the PL spectrum by up to 60 nm.[18] Tsai et al. reported on an encapsulated RPP solar cell that was photostable for over 2250 h under constant, standard (AM1.5G) illumination, while nonencapsulated solar cells lost about 40% of their efficiency in the meantime.[7] From a comparison between thin films and exfoliated flakes, Blancon et al. stressed the importance of low energy electronic edge states for exciton dissociation in RPPs with more than three layers.[19] The fundamental understanding of light-induced local and surface structural changes is therefore important to improve the lifetime of perovskite-based devices and to effectively tailor their photophysical properties.

Up until now, most photostability studies have been focused on 3D perovskites, while the mechanisms involved in

Dr. H.-H. Fang, Dr. J. Yang, S. Adjokatse, M. E. Kamminga,
Prof. J. Ye, Dr. G. R. Blake, Prof. M. A. Loi
Zernike Institute for Advanced Materials
University of Groningen
Nijenborgh 4, 9747 AG Groningen, the Netherlands
E-mail: J.Yang@rug.nl; M.A.Loi@rug.nl
Dr. S. X. Tao
Center for Computational Energy Research
Department of Applied Physics
Eindhoven University of Technology
P. O. Box 513, 5600 MB Eindhoven, the Netherlands
Prof. J. Even
Fonctions Optiques pour les Technologies de l'Information
FOTON UMR 6082
CNRS
INSA de Rennes
Rennes 35708, France

**ADVANCED
SCIENCE NEWS**
www.advancedsciencenews.com

**ADVANCED
FUNCTIONAL
MATERIALS**
www.afm-journal.de

the light-induced degradation of layered perovskites remains elusive.[7] From both application and fundamental standpoints, the response of layered perovskites under light is particularly interesting, and may be also helpful for understanding the mechanisms of light-induced degradation in their 3D counterparts, which is still under intense debate.[20–23]

In this work, ultrathin $(PEA)_2PbI_4$ crystalline flakes are used as model to investigate the response of layered perovskite lattice to light irradiation. Nanoflakes can be produced with lateral dimensions of tens of micrometers and atomically flat surfaces. This enables fundamental studies to be performed of the reaction pathway of layered perovskites under the excitation of light. By using in situ experimental techniques such as atomic force microscopy (AFM) and confocal laser scanning microscopy (CLSM), we correlate the evolution of the morphology of the flakes with their PL. The structural evolution from a 2D perovskite lattice to layered PbI_2 is monitored. Light-induced degradation of the 2D perovskite lattice occurs via the release of PEA + HI from the edges of the flakes and the surfaces, where the inorganic layers are broken down. The role of the laser wavelength on the degradation is further investigated. It is demonstrated that the crystals are stable under off-resonant excitation. The experimental data show that a lower energy is required to break the PbI_6 octahedra than for their 3D counterparts. The evolution of the layered perovskite to PbI_2 under resonant photoexcitation provides important mechanistic insights into the light-induced reaction pathways. By encapsulating the layered materials with polycarbonates and hexagonal boron nitride layers, the photostability of the perovskite is enhanced.

2. Results and Discussion

2.1. Layered Perovskite

The general formula of 2D multilayered RPPs is $(RNH_3)_2A_{n-1}M_nX_{3n+1}$ (n = 1, 2, 3, 4... is the number of perovskite layers), where RNH_3 is a large aliphatic or aromatic alkylammonium spacer cation, such as 2-phenylethylammonium (PEA).[24–27] Other types of multilayered halide perovskites have recently emerged with similar attractive optoelectronic properties, including structures with an alternating arrangement of two different cations in the interlayer space and a slightly different chemical formula.[28] These hybrid multilayered halide perovskites contain MX_6 octahedra. In 2D monolayered compounds each metal cation shares halide ions only with its neighboring in-plane metal cations. The organic molecules form a layer with a low dielectric constant whereas the metal halide layers possess a high dielectric constant,[29] and in addition a strong quantum confinement effect is present leading to a direct band gap and a type-I superlattice structure where barriers and wells alternate with each other.[30] In these layered perovskites, the excitonic effect is greatly enhanced due to the strong dielectric confinement and Coulomb interaction,[25,31–34] giving rise to bright PL at room temperature. These features make them attractive for optoelectronics, especially for light emitting diodes (LEDs) and lasers.[31,35–41]

The $(PEA)_2PbI_4$ crystals were synthesized by the antisolvent vapor-assisted crystallization method.[42] Briefly, a mixture of (PEA)I and PbI_2 with a molar ratio of 2:1 was dissolved in N,N-dimethylformamide (DMF). Dichloromethane (DCM) was used as an antisolvent, which was slowly diffused into the solution containing the crystal precursors. Using this method, high-quality, millimeter-sized $(PEA)_2PbI_4$ single crystals are obtained within 2 days.

Ultrathin crystalline nanoflakes of $(PEA)_2PbI_4$ are produced by a mechanical exfoliation technique as already successfully applied to other van der Waals materials, such as graphene and transition-metal dichalcogenides (TMDs).[43] **Figure 1** shows optical microscopy images of $(PEA)_2PbI_4$ flakes obtained by mechanical exfoliation. Typical flakes are found to have lateral dimensions of tens of microns. Due to diffraction between the top and bottom facets, the perovskite nanoflakes show varied colors depending on the thickness,[44] which can be correlated with the optical images and atomic force microscopy. The exfoliated flakes were further characterized by powder X-ray diffraction (XRD) (Figure S1, Supporting Information). Bragg reflections with high intensity were observed at 10.9°, 16.3°, 21.8°, and 27.3°, which can be well indexed as the (004), (006), (008) and (0010) planes of $(PEA)_2PbI_4$ with the $P2_1/c$ space group (Table S1, Supporting Information).[45]

2.2. Dynamical Degradation of Layered Perovskite

The $(PEA)_2PbI_4$ crystalline flakes are reasonably stable in air. Surprisingly, we found that the surface roughens when characterizing them by AFM microscopy with the white illumination on. The microscope image shown in Figure 1B (Figure S2, Supporting Information) also shows a color variation after prolonged exposure to a blue laser (488 nm, 120 mW cm^{-2}). We attribute the color change to variations in the thickness of the perovskite flakes as a different color is the signature of a different thickness for many layered materials when positioned on dielectrics.[44] AFM measurements were performed to investigate the morphological transformation of the samples, before and after 15 min of illumination with the 488 nm laser source (Figure S3, Supporting Information). Figure 1C,D shows AFM images before and after light illumination, respectively. The corresponding height profiles obtained from Figure 1C,D (Figure 1E) shows that the thickness of the $(PEA)_2PbI_4$ flakes measured at the center of the surface decreased from 210 to 155 nm after illumination with the 488 nm laser. Figure 1F shows the thicknesses of the illuminated samples (after 15 min of illumination) as a function of their initial thicknesses. The reduction in thickness is as large as 90 nm. It is interesting to note that the ratio of the thicknesses before and after illumination is ≈0.42 for thin flakes (<100 nm). We speculate that such a large reduction in thickness originates from the transformation of $(PEA)_2PbI_4$ to PbI_2. The organic molecules are removed from the lattice during the illumination process, leaving only PbI_2 layers. This is confirmed by the progressive appearance of new XRD peaks at 2θ = 12.99° and 26.24° (Figure S1, Supporting Information). These two new peaks
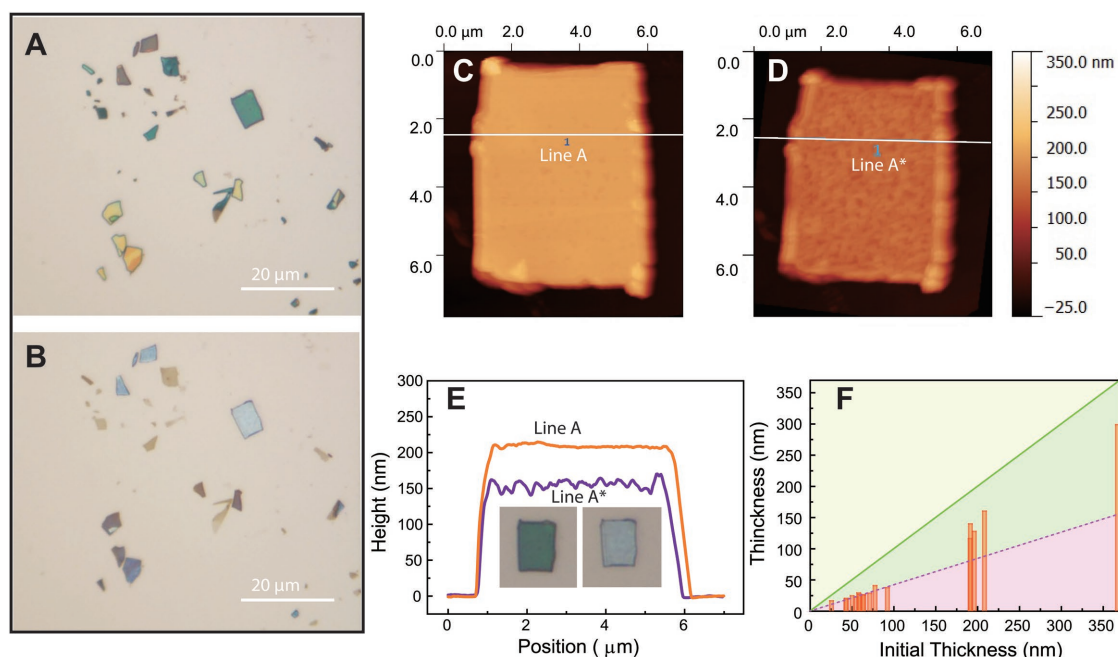
Figure 1. A) Color optical image of mechanically exfoliated flakes of $(PEA)_2PbI_4$ single crystals on a Si substrate. B) Optical image of flakes of $(PEA)_2PbI_4$ single crystals taken after illumination with a 488 nm laser for 20 min, showing color changes. AFM height images of a $(PEA)_2PbI_4$ flake are shown C) before and D) after illumination with the 488 nm laser. E) Corresponding height profiles obtained along the lines shown in (C) and (D). The thickness of the $(PEA)_2PbI_4$ flakes decreases after illumination with the 488 nm laser. F) Thickness of illuminated samples as a function of their initial thickness. The slope of the green line is 1, and the slope of the violet dashed line is 0.42.

are attributed to the (001) and (002) planes of PbI_2,[46] respectively. For ultrathin flakes, $(PEA)_2PbI_4$ may be completely converted to PbI_2. In fact, the thickness ratio of 0.42 agrees well with the lattice constant ratio of the two phases along the c axis (6.78 Å for PbI_2, and 16.13 Å for $(PEA)_2PbI_4$), further substantiating this conclusion.

Figure 2A shows optical images of mechanically exfoliated flakes of $(PEA)_2PbI_4$ single crystals on a glass substrate after exposing the sample to the laser (continuous wave laser, 488 nm, $120\,mW\,cm^{-2}$) for different lengths of time. Before illumination, it is noted that the surface color of the flakes of $(PEA)_2PbI_4$ is uniform, and the corresponding fluorescence microscopy image shows emission with more than 1250 counts at the center of the crystal (Figure 2C). Interestingly, the emission intensity at the crystal edges is much higher than at the center of the crystal, as high as 8800 counts, as shown in Figure 2C. This can be attributed to an optical waveguide effect of photons confined in the flakes, which propagate till the edges. After illumination for 2 min, the color of the largest flake changes from yellow to green, and several microstructures appear on the surface. We attribute the simultaneous color change to a thickness change. It is noted that the emission intensity slightly decreases to 1100 counts at the center of the crystal, while it is strongly reduced at the edges to 430 counts at point A and less than 2000 counts at point B (Figure 2C). After longer laser treatment for 4.5 min, the color of the optical image is further changed with a strong degree of surface inhomogeneity and significantly lowered emission intensity. In contrast to the initial PL intensity profile, the emission intensity at the edges is much smaller than at the center. After

further illumination up to 7 min, the color of the largest crystal becomes uniform again, but the emission is totally quenched. This suggests that the surface of $(PEA)_2PbI_4$ is completely transformed to PbI_2, which has a very low PL quantum efficiency.

To monitor the morphology changes, in situ investigation of the perovskite surface was performed by AFM. **Figure 3**A shows a surface image of a freshly exfoliated $(PEA)_2PbI_4$ flake that was not exposed to the laser. The image shows uniform, flat areas separated by step-like changes in height, typical of layered materials with a vertical stacking axis. The corresponding height profile (Figure 3C) reveals a 1.7 nm step, which is consistent with the distance between the inorganic layers along the c-axis of the crystal structure (a single unit cell (i.e., a bilayer) of the bulk material is 3.2 nm in thickness). The freshly exfoliated flakes possess highly smooth surfaces with a surface roughness of ≈ 0.45 nm (root mean square height fluctuation). After 10 s of illumination with a laser diode (405 nm, 50 mW, $1.5\,cm^2$), the roughness is significantly increased to 2.80 nm with the creation of apparent surface defects (Figure 3B). The AFM cross-sectional height profile analysis indicates that the depth of these surface nanodefects is as low as 10 nm, which suggests that about five layers of the inorganic lattice have been broken down during the illumination process.

On the basis of the above described observation, we posit that $(PEA)_2PbI_4$ is transformed into PbI_2 and other volatile components under illumination. **Figure 4**A schematically shows the proposed light induced degradation process, which can be expressed as the following
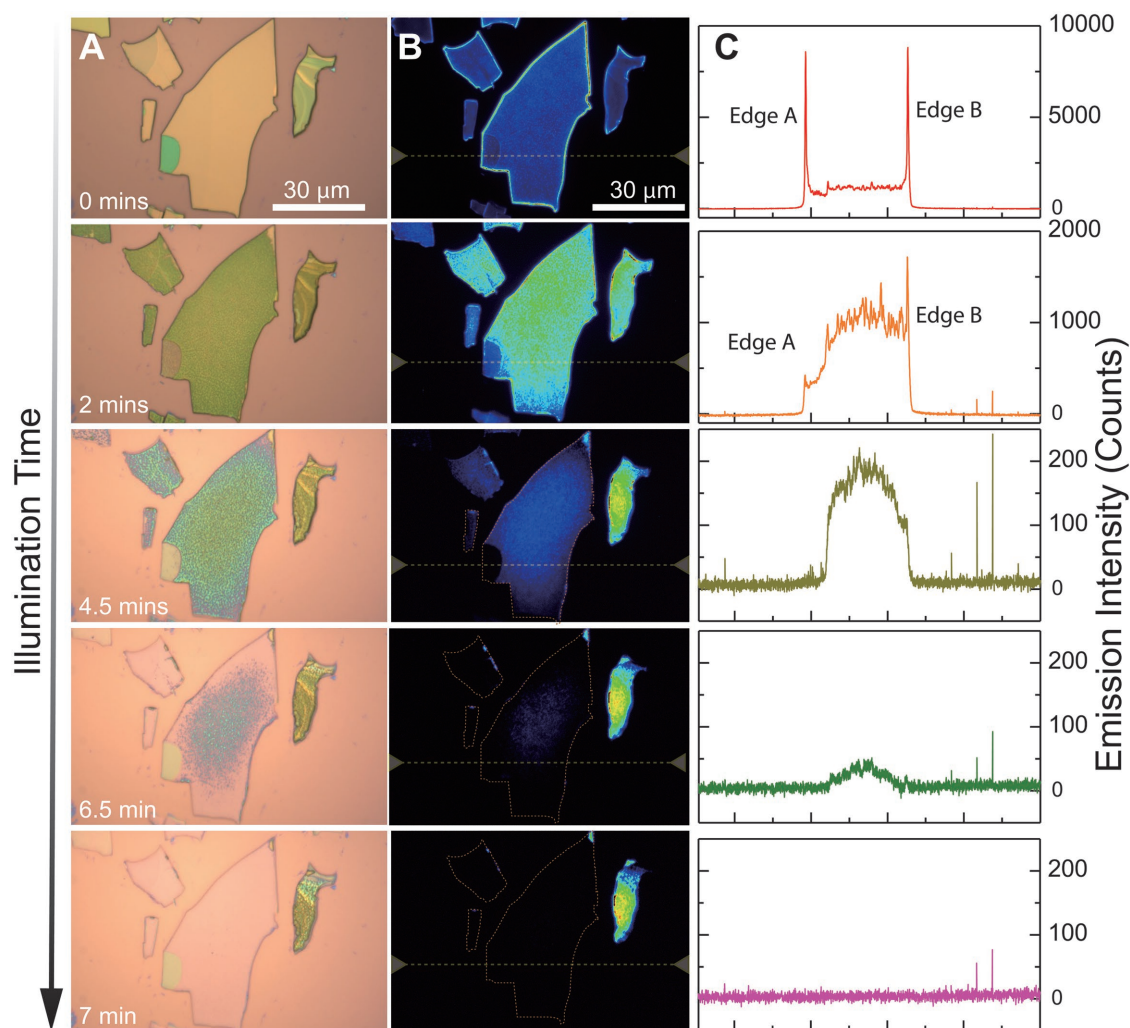
$$(PEA)_2\,PbI_{4\,solid} \rightarrow PbI_{2\,solid} + \left[PEA^+ + I^-\right] \rightarrow PbI_{2\,solid} + PEA_{gas} + HI_{gas}$$

ADVANCED
SCIENCE NEWS
www.advancedsciencenews.com

ADVANCED
FUNCTIONAL
MATERIALS
www.afm-journal.de

Figure 2. A) Colour optical images of mechanically exfoliated flakes of (PEA)$_2$PbI$_4$ single crystals on a glass substrate taken at various illumination times (with a continuous wave laser, 488 nm, 120 mW cm^{-2}). B) Photoluminescence intensity mapping of the same (PEA)$_2$PbI$_4$ single-crystal flakes at illumination times corresponding to the images in (A) (the PL intensity scale is normalized to 0–1 in all images). C) The corresponding emission intensity profiles obtained along the dashed lines in (B).

The volatile PEA and HI are initially released from the corroded edges and surface, leaving PbI$_2$ residue.

To further probe the crystal transformation pathway, we characterized the evolution of the flakes using CLSM. An argon ion laser (488 nm) was used for raster scanning the sample in order to trigger the degradation process and simultaneously image the evolution of the light-induced PL image. Figure 4B–G presents CLSM images taken at different laser scanning times (see Video S1 in the Supporting Information, for the dynamical evolution of CLSM images). Prior to laser scanning, the crystals showed uniform PL from the surface. After 30 min of laser scanning, irregular PL image with lower emission intensity at the edges of the flake as well as at cracks was clearly observed. This is likely an indicator of the structural transformation of (PEA)$_2$PbI$_4$ to PbI$_2$, which correlates with the color changes observed by wide-field optical microscopy (Figure 2). The variation of the PL intensity across the surface can be ascribed to both a heterogeneous distribution of PbI$_2$ (as shown in Figure 3B) or to the introduction of surface traps. With continued scanning, domains in which the PL was quenched (dark regions) appeared and became more widespread. Eventually, the PL became quenched from almost the entire crystal after 7 h of laser scanning.

2.3. Mechanism of Light Induced Degradation

Previous studies have reported that MAPbI$_3$ decomposes into PbI$_2$ and other components under exposure to heat, light and water.[4,21,47] In order to compare with (PEA)$_2$PbI$_4$, the evolution of the PL of MAPbI$_3$ single crystals was investigated as a function of illumination time using the 488 nm laser and the same excitation power as for (PEA)$_2$PbI$_4$. Although a degree of uneven PL was observed across the surface of MAPbI$_3$ single crystals, with some bright spots located at random, the variation in the local PL after 5.5 h of laser scanning was much smaller compared to the layered perovskite (see Figure S4 in the Supporting Information). Notably, the overall PL intensity is increased by 4–5 times, which is in striking contrast with the
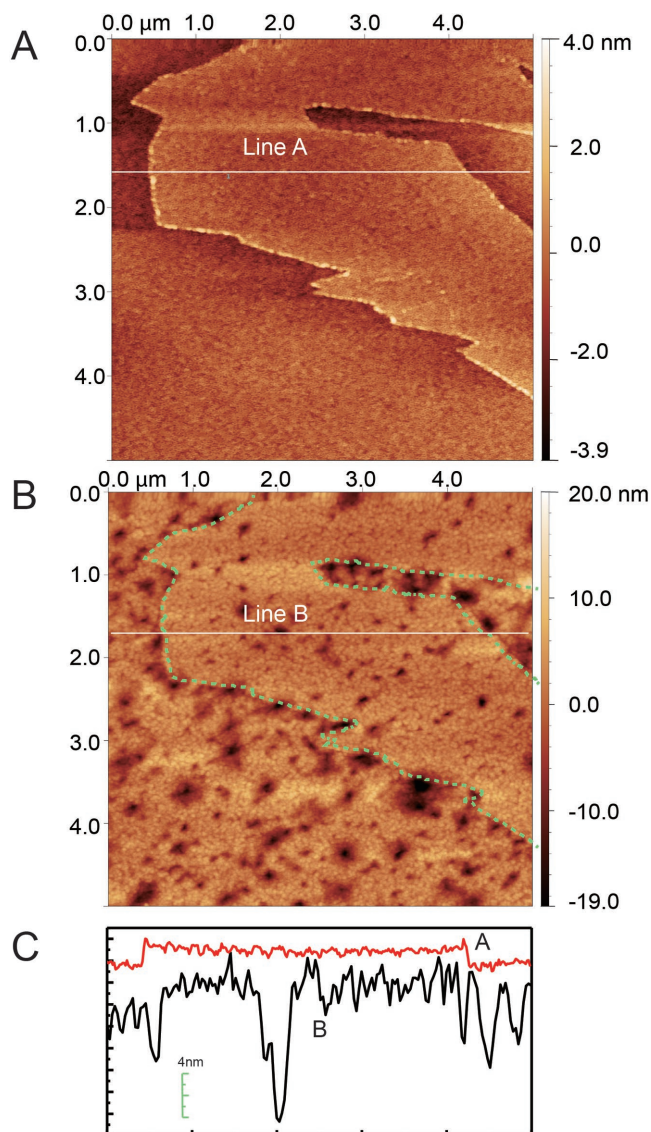
Figure 3. A) AFM images of the freshly cleaved surface of a $(PEA)_2PbI_4$ flake. B) AFM image of the surface of the same flake after 10 s illumination by a 405 nm laser diode. C) Corresponding height profiles obtained along the white lines shown in (A) and (B).

layered perovskite. This suggests that the atomic mechanism of light induced degradation in layered perovskites is essentially different from their 3D counterparts.

PL and time-resolved photoluminescence (TRPL) measurements were further performed to gain insight into the light-illumination effect on the exciton recombination. PL spectra and TRPL curves for the pristine samples and for the same samples after illumination under a 400 nm femtosecond laser are shown in **Figure 5**. The freshly cleaved crystals show quantum yield as high as 86%. After illumination for 60 min, the emission peak is slightly blue-shifted and becomes ≈500 times lower in intensity. The pristine sample displays PL dynamics with a fast component fitted by $t_1 = 5$ ns and a slow component with $t_2 = 45$ ns. The fast component is attributed to surface recombination, which is related to the laser-induced

surface transformation and creation of traps, while the slow component is considered to be the intrinsic exciton recombination lifetime. The fast component substantially increases and becomes dominant in the PL dynamics after extended illumination, with lifetime $t_1 = 0.5$ ns (99.5 %) and a slow component with $t_2 = 28$ ns (0.5%). We attribute this behavior to the increased number of traps due to structural transformation at the surface.

At this point, it is natural to ask whether the degradation by irradiation reported here is due to localized heating by the laser, as hybrid perovskites are known to be unstable under high temperature. We observed that the PL quenching effect and spatial heterogeneity became negligible when the flakes are scanned using 543 and 632 nm lasers, which correspond to off-resonant excitation (see Figure S5, Supporting Information). After 2 h of scanning, the crystals showed little change in the PL maps. In contrast, the PL was significantly quenched for the 488 nm laser. Due to the strong resonant absorption, laser illumination with energy larger than the bandgap may induces temperature increase at crystal surface. We have therefore monitored the temperature variation with a fine wire thermal coupler, which touches the surface of a 1.5×1 mm crystal. The temperature increase from 21.5 °C to 25 °C, when the sample is illuminated with the laser at 180 mW cm^{-2} for 3 min. Furthermore, thermogravimetric (TG) and differential scanning calorimeter (DSC) measurements were performed to determine the temperature stability of the material. The measurements (see Figure S6, Supporting Information) reveal that $(PEA)_2PbI_4$ is thermally stable up to 250 °C, which is comparable with what has been reported for $MAPbI_3$ (240 °C).[48] The PL also shows high stability to elevate temperature. Negligible PL quenching is observed in flakes that have been kept at 100 °C for 1 hour (see Figure S7, Supporting Information). Thus, the heat caused by the laser may not be the direct reason for the degradation. However, the temperature plays important role on the photostability of layered perovskite. We find that the degradation is accelerated when the 2D flakes are illuminated with a 488 nm laser light while kept at 100 °C. In this situation the PL intensity drops by 90% in 3 s. The PL intensity remains 50% after 30 min illumination, when the sample is kept at −73 °C, demonstrating that the degradation process is retarded at low temperature. Therefore, we can conclude that the resonant photoexcitation triggers the degradation process, while the high temperature enhances the volatility of the organic anions.

Recent reports have demonstrated that above-gap photoexcitation induces significant rotational sublattice disorder of the iodine–lead octahedra in $MAPbI_3$, associated with changes of the I—Pb—I bond angles.[49,50] The space group of $(PEA)_2PbI_4$ was previously reported to be C2/m.[51] As shown in **Figure 6**, the local geometry within the PbI_6 octahedra differs in 3D and 2D perovskites. It is related to a different organic-inorganic stacking pattern in $MAPbI_3$ (Figure 6A) and $(PEA)_2PbI_4$ (Figure 6C). Within $MAPbI_3$, due to the 3D periodic arrangement of the PbI_6 octahedra, the deviations of the Pb—I bond lengths are small, indicating a rather similar bonding strength for all Pb—I bonds (Figure 6B). On the contrary, two types of Pb—I bonds can be identified in 2D $(PEA)_2PbI_4$ (Figure 6D): i) Pb—I

**ADVANCED
SCIENCE NEWS**
www.advancedsciencenews.com

**ADVANCED
FUNCTIONAL
MATERIALS**
www.afm-journal.de

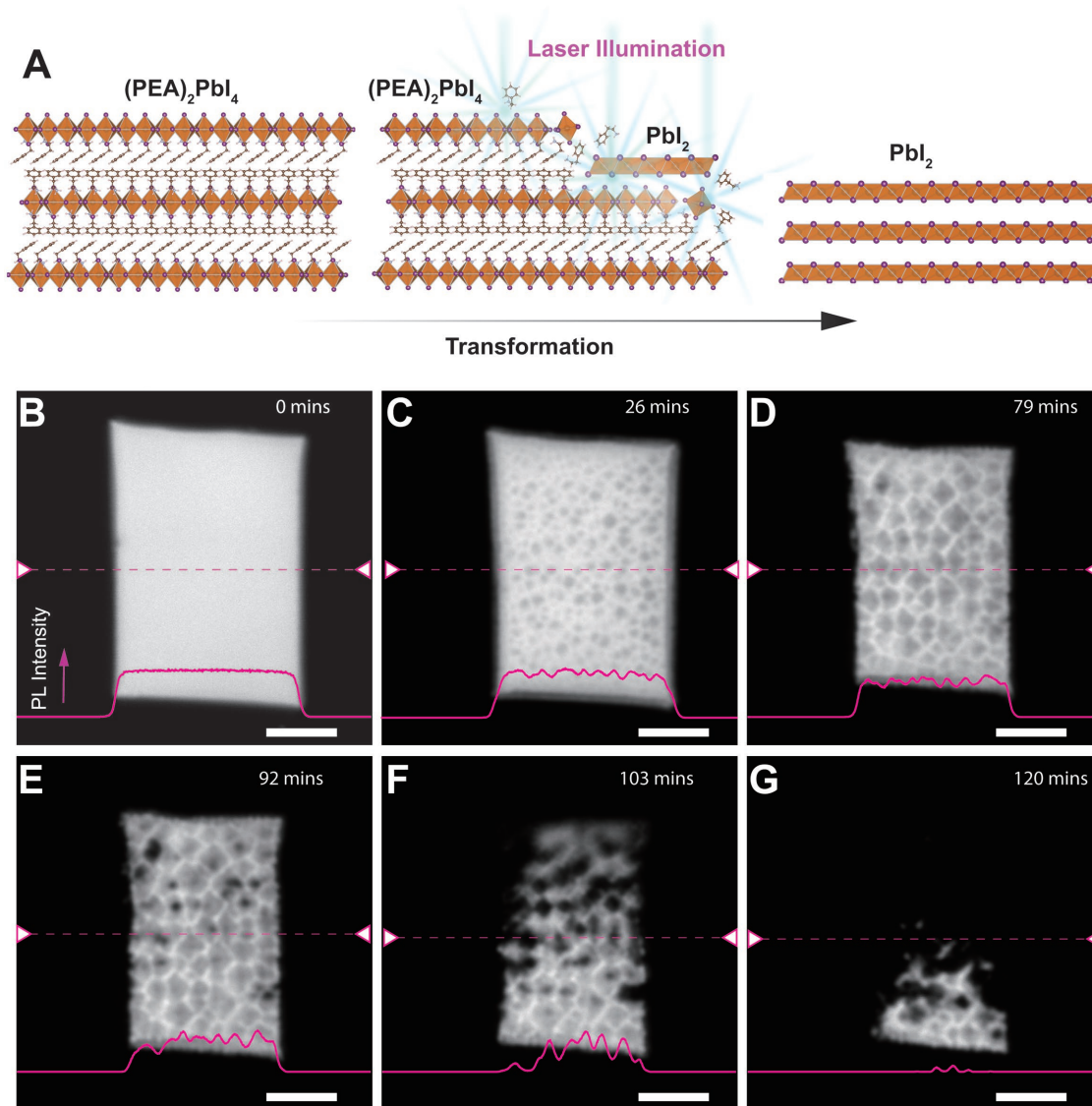**Figure 4.** A) Schematic illustration of the structural evolution from $(PEA)_2PbI_4$ to PbI_2 under resonant excitation. B–G) Confocal microscopy images of a flake at increasing illumination time under a 488 nm laser.

bonds in the plane of the inorganic framework (*ab* plane); ii) dangling Pb—I bonds along the *c* axis, where the I^- anions closely interact with the PEA^+ cations. The in-plane Pb—I bond lengths are very similar to those in 3D $MAPbI_3$. However, the out-of-plane Pb—I bonds are significantly longer, indicating a lower degree of covalent bonding and therefore weaker Pb—I bonds. As demonstrated experimentally and discussed above, the degradation at the surface of $(PEA)_2PbI_4$ is much faster than that of $MAPbI_3$, pointing to the conclusion that the Pb—I bonds along the *c* axis are much more vulnerable and easier to activate than the Pb—I bonds lying in the *ab* plane.

Our observations also show that the laser-induced structural transformation at the edges of crystalline flakes is much faster than that at the surface. A possible scenario is that upon resonant photoexcitation, iodine–lead octahedra is distorted, and volatile organic cations may start to diffuse out from the edges,

initiating a collapse of the perovskite framework into PbI_2. This leads to a new exposure of the organic cations at the newly formed steps (see Figure 4A), which again allows the volatile component to escape easily from the crystal. In the meantime, the excitation/breaking of a large number of Pb—I bonds at the surface creates a lot of vacancies and local disorder, facilitating the further release of PEA and HI from the surface. This is in contrast to the phenomena observed in 3D $MAPbI_3$ by Fan et al., where the degradation occurs in a sequential layer-by-layer manner.[21] From our experimental observations, we may infer that the release of the organic cations is much easier in layered perovskites, especially at the edges. Recently, increasing number of research groups have been developing devices based on 2D/3D mixed perovskite.[10,52] These composites are partly retaining some of the features of the 2D and of the 3D constituents, giving an overall enhanced stability.
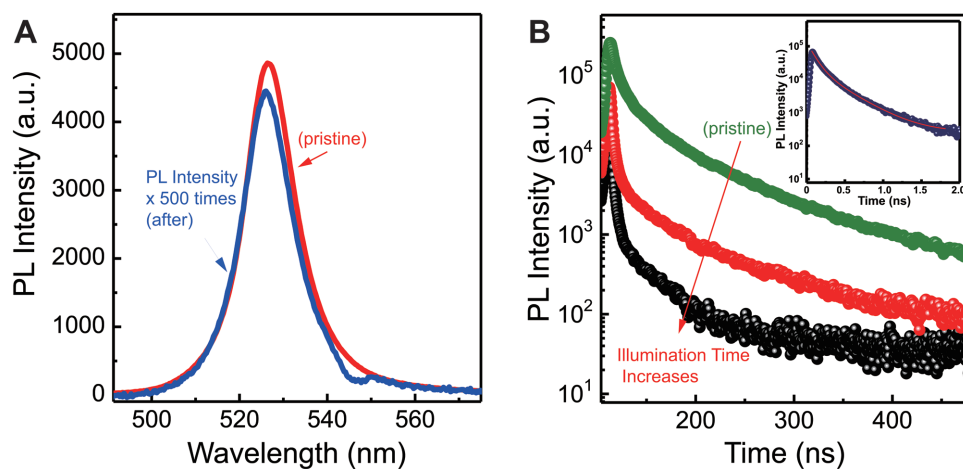
Figure 5. A) Photoluminescence spectra before (red curve) and after (blue curve) illumination with a pulsed laser at 400 nm for 96 min (0.18 µJ cm^{-2}). For the purpose of comparison, the intensity of the PL spectra after illumination (blue curve) is multiplied by a factor of 500. B) Time-resolved photoluminescence decay of (PEA)$_2$PbI$_4$ after different illumination times (green-freshly cleaved sample, red 47 min, black 96 min) using a 400 nm femtosecond laser. The fast component becomes dominant after prolonged illumination.

2.4. Encapsulation for Improved Photostability

This new insight suggests that it would be possible to suppress the degradation process by confining the organic cations. To this end, we employed a thin layer of hexagonal boron nitride (hBN) and/or polycarbonates to protect the 2D perovskite flakes. **Figure 7**A presents a schematic diagram of the fabrication of encapsulated samples by vertically stacking a hBN layer on top of (PEA)$_2$PbI$_4$ flakes using a mechanical stacking method. Figure 7B shows a bright-field microscopy image of several (PEA)$_2$PbI$_4$ flakes, one which is fully covered by a mechanically exfoliated hBN flake (point B), and another that is half covered (point C). The perovskite flakes covered by hBN emit strong green light in similar fashion to the non-encapsulated samples (Figure 7D, and Video S2 in the Supporting Information), when initially under illumination of a 488 nm laser. After 30 min of continuous illumination, the emission from the nonencapsulated perovskites is completely quenched, whereas perovskite flakes that are fully encapsulated by hBN maintain uniform, intense emission (60% of the initial value, see Figure 7E). Little change in color is observed for encapsulated flakes when investigated under the bright-field microscope, as indicated at point A in Figure 7C, whereas exposed flakes show dramatic changes in color, suggesting that they undergo structural transformation as discussed above. Interestingly, the partially encapsulated crystals remain emissive. However, their edges are corroded, again suggesting the important role of the edges in the degradation process. The atomically flat h-BN layers serve as an excellent protection for the perovskite. This is attributed to the confinement effect of h-BN, which prevents PEA and HI from escaping from the crystal. Various layered perovskites have been demonstrated to show interesting features, such as direct bandgaps and high photoluminescence quantum yield. We note that the encapsulation of 2D dichalcogenide slabs with h-BN has also been used successfully.[53] The combination of ultrathin layers of 2D perovskites with TMDCs or graphene may offer new potential to develop 2D heterostructures and devices. Layered perovskites encapsulated with

polycarbonates also show excellent photostability (Figure S8, Supporting Information). The PL intensity of polycarbonate encapsulated sample retains 55% of its initial value after 30 min illumination and reduces to about 40% after 80 min (Figure S9, Supporting Information). Therefore, encapsulation could be a feasible way to enhance the stability of large-scale devices.

3. Conclusion

In summary, the light-induced degradation of the layered perovskite (PEA)$_2$PbI$_4$ has been investigated. By exposing the crystalline flakes to a laser, we observed the evolution of the structure from (PEA)$_2$PbI$_4$ to PbI$_2$. Upon resonant photoexcitation, volatile organic cations start to diffuse out from the edges, and at the surface where the inorganic layers are broken down. Our comparative CLSM study under laser scanning with different wavelengths suggests that above-gap photoexcitation plays an important role in triggering the breakdown of the framework of (PEA)$_2$PbI$_4$. The light-induced degradation can be significantly suppressed by an efficient encapsulation design using 2D semiconductors and/or polycarbonates. These results afford unprecedented opportunities for combining layered perovskites with other 2D materials and thereby customizing new functionalities in van der Waals heterostructures.

4. Experimental Section

Materials: C$_6$H$_5$C$_2$H$_4$NH$_3$I (PEAI) (>98%) was purchased from TCI Europe N.V. PbI$_2$ (99.999%), DMF (99.8%), and DCM (99.8%) were acquired from Sigma-Aldrich. All the materials were used as received without further purification. Single crystals of (PEA)$_2$PbI$_4$ were synthesized by the antisolvent vapor–assisted crystallization (AVC) method. (PEA)$_2$PbI$_4$ precursor solutions were prepared by dissolving PbI$_2$ and PEAI in DMF (1:2 molar ratio). A precursor solution (1 mol L^{-1}) was poured into a small vial and then placed in a bigger vial, which contained the antisolvent, DCM. After 48 h, millimeter-sized rectangular-shaped
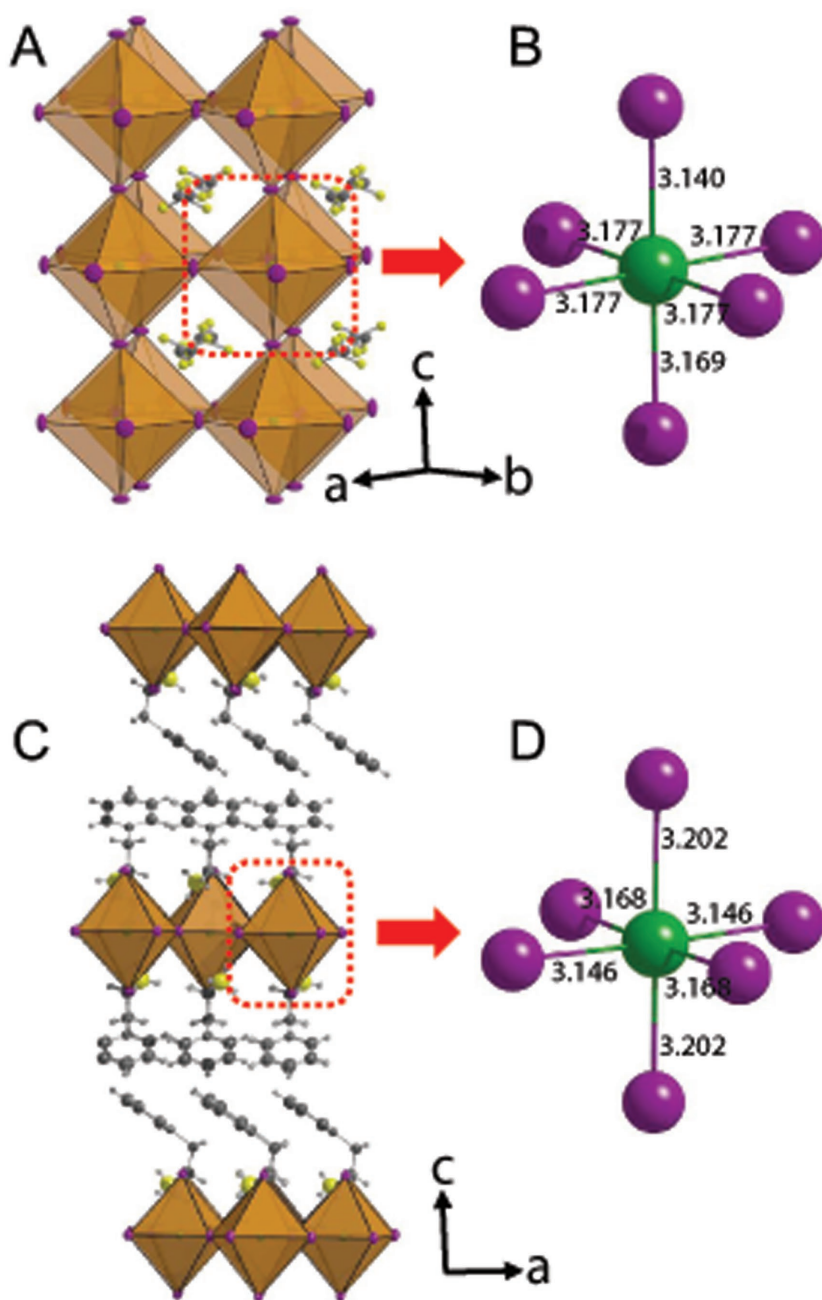
**ADVANCED
SCIENCE NEWS**
www.advancedsciencenews.com

**ADVANCED
FUNCTIONAL
MATERIALS**
www.afm-journal.de

Figure 6. Comparison of structural properties of 3D MAPbI$_3$ and 2D (PEA)$_2$PbI$_4$. Crystal structure of A) MAPbI$_3$ with tetragonal structure and C) (PEA)$_2$PbI$_4$ with monoclinic structure; bond lengths (numbers in black in units of Å of Pb—I in the inorganic octahedron at 200 K are shown for B) MAPbI$_3$ and D) (PEA)$_2$PbI$_4$.

Characterization: Atomic force microscopy images were acquired in tapping mode using a Veeco Dimension V scanning probe microscope under ambient conditions. Bright field microscope images and dark field microscope images were captured by a home-built microscope. For the dark field images, a defocused, spatially homogeneous 488 nm continuous-wave (CW) laser was used as excitation. Confocal laser scanning microscopy was performed with an experimental set up based on an inverted Nikon Eclipse Ti microscope. Three single line continuous wave lasers (488, 543, and 632 nm) are available as the excitation source for laser scanning. The sample images were recorded using a set of photomultiplier tubes (PMT) covering a spectral detection range of 460–750 nm. The spatial resolution achievable is calculated using the equation $d = 0.46\lambda/NA$, where λ is the excitation wavelength and NA is the numerical aperture of the microscope objective.

Photoluminescence Spectroscopy: The photoluminescence measurements were performed using the second harmonic (400 nm) of a Ti: sapphire laser (repetition rate, 76 MHz; Mira 900, Coherent) to excite the samples. The illumination power density was adjusted by using neutral density filters. The excitation beam was spatially limited by an iris and focused with a 150 mm focal length lens. Emitted photons were collected with a lens and directed to a spectrograph. For the time-resolved photoluminescence measurement, a pulse picker was used to divide the Ti: sapphire oscillator frequency. Steady-state spectra were collected using a Hamamatsu EM-CCD camera and time-resolved traces were recorded using a Hamamatsu streak camera.

Crystal Structure: Powder X-ray diffraction was performed at ambient conditions. The X-ray data were collected using a Bruker D8 Advance diffractometer in Bragg-Brentano geometry and operating with Cu Kα radiation source ($\lambda = 1.54$ Å) and Lynxeye detector. Single-crystal XRD measurements were performed using a Bruker D8 Venture diffractometer operating with Mo Kα radiation and equipped with a Triumph monochromator and a Photon100 area detector. A 0.3 mm nylon loop and cryo-oil were used to mount the crystals and a nitrogen flow from an Oxford Cryosystems Cryostream Plus was used to cool down the crystals. Data processing was done using the Bruker Apex II software and the SHELX97 software was used for structure solution and refinement.[55]

Calorimetry Measurements: Differential scanning calorimetry (DSC) measurements were performed using a TA-instruments STD 2960. An Al crucible was used to measure a powder sample of 25.77 mg over a temperature range of 60 to 500 K at a rate of 5 K min^{-1} under a 100 mL min^{-1} argon flow.

Encapsulation of Layered Perovskite: For polycarbonate encapsulation, the polycarbonate was dissolved in chloroform. The solution was then blade coated on the substrates with (PEA)$_2$PbI$_4$ flakes. For encapsulation with hBN, layers of (PEA)$_2$PbI$_4$ were exfoliated onto a silicon substrate. The hBN crystals used for the exfoliation was purchased from HQ Graphene. In the meantime, few-layer hBN was exfoliated onto another silicon substrate. A PDMS (polydimethylsiloxane) stamp attached with polycarbonate was positioned to pick up the layer of hBN and was then brought into contact with the perovskite layer. The polycarbonate stack was released by heating the substrate to 85 °C. After transfer, the polymer stack was dissolved in chloroform.

orange crystals started to grow in the small vial. (PEA)$_2$PbI$_4$ flakes are exfoliated onto a substrate from a small piece of (PEA)$_2$PbI$_4$ crystal by the commonly used mechanical exfoliation ("scotch-tape") technique.[54] The (PEA)$_2$PbI$_4$ crystal was stuck on a scotch tape. Then the part of tape with the (PEA)$_2$PbI$_4$ crystal was repeatedly folded and unfolded for several times until (PEA)$_2$PbI$_4$ crystal covered a large portion of the tape. A piece of SiO2/Si wafer was placed back-side onto the (PEA)$_2$PbI$_4$ crystal on the tape, and pressed to the tape for several seconds. After gently removing the tape, small thin flakes of (PEA)$_2$PbI$_4$ crystals were left on the surface of SiO2/Si wafer.
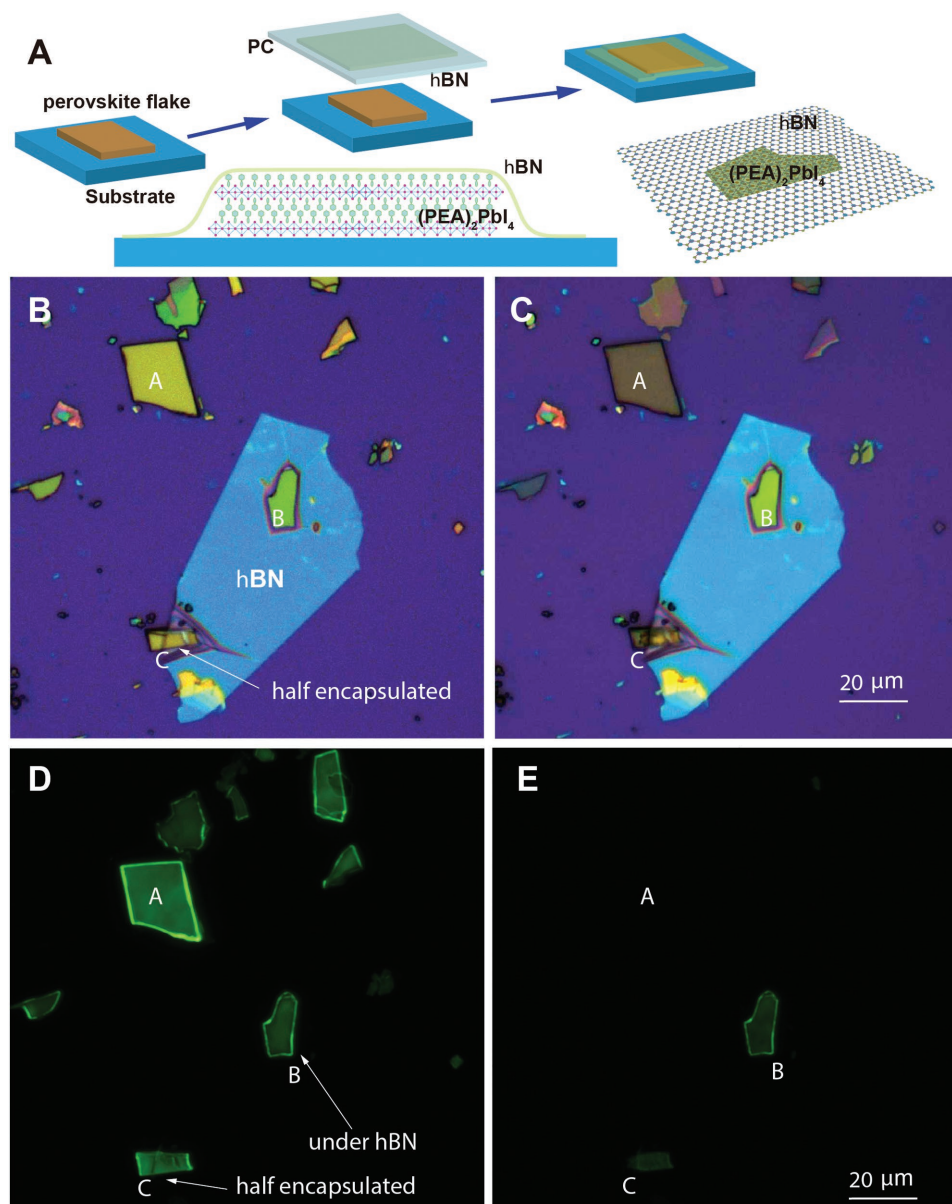
Figure 7. A) Schematic of the hBN-perovskite stack fabrication process for encapsulation of perovskite nanoflakes. Bright-field microscopy images of hBN/(PEA)$_2$PbI$_4$ heterostructure before B) and after C) treatment with a 488 nm laser for 30 min. The substrate is SiO$_2$/Si. Fluorescence images of (PEA)$_2$PbI$_4$ are shown before D) and after E) treatment with the 488 nm laser for 30 min. The encapsulated perovskite retains strong emission intensity after treatment, while the emission for the nonencapsulated perovskite is completely quenched.

Supporting Information

Supporting Information is available from the Wiley Online Library or from the author.

Conflict of Interest

The authors declare no conflict of interest.

[1] M. Saliba, T. Matsui, K. Domanski, J.-Y. Seo, A. Ummadisingu, S. M. Zakeeruddin, J.-P. Correa-Baena, W. R. Tress, A. Abate, A. Hagfeldt, M. Grätzel, *Science* **2016**, *354*, 206.

[2] D. Zhao, Y. Yu, C. Wang, W. Liao, N. Shrestha, C. R. Grice, A. J. Cimaroli, L. Guan, R. J. Ellingson, K. Zhu, X. Zhao, R.-G. Xiong, Y. Yan, *Nat. Energy* **2017**, *2*, 17018.

[3] K. Zheng, Q. Zhu, M. Abdellah, M. E. Messing, W. Zhang, A. Generalov, Y. Niu, L. Ribaud, S. E. Canton, T. Pullerits, *J. Phys. Chem. Lett.* **2015**, *6*, 2969.

[4] J. Yang, B. D. Siempelkamp, D. Liu, T. L. Kelly, *ACS Nano* **2015**, *9*, 1955.

[5] G. Divitini, S. Cacovich, F. Matteocci, L. Cinà, A. Di Carlo, C. Ducati, *Nat. Energy* **2016**, *1*, 15012.

[6] S. Yang, Y. Wang, P. Liu, Y.-B. Cheng, H. J. Zhao, H. G. Yang, *Nat. Energy* **2016**, *1*, 15016.

[7] H. Tsai, W. Nie, J.-C. Blancon, C. C. Stoumpos, R. Asadpour, B. Harutyunyan, A. J. Neukirch, R. Verduzco, J. J. Crochet, S. Tretiak, L. Pedesseau, J. Even, M. A. Alam, G. Gupta, J. Lou, P. M. Ajayan, M. J. Bedzyk, M. G. Kanatzidis, A. D. Mohite, *Nature* **2016**, *563*, 312.

[8] J. Byun, H. Cho, C. Wolf, M. Jang, A. Sadhanala, R. H. Friend, H. Yang, T.-W. Lee, *Adv. Mater.* **2016**, *28*, 7515.

[9] H. Tsai, W. Nie, J.-C. Blancon, C. C. Stoumpos, C. M. M. Soe, J. Yoo, J. Crochet, S. Tretiak, J. Even, A. Sadhanala, G. Azzellino, R. Brenes, P. M. Ajayan, V. Bulović, S. D. Stranks, R. H. Friend, M. G. Kanatzidis, A. D. Mohite, *Adv. Mater.* **2018**, *30*, 1704217.

[10] G. Grancini, C. Roldán-Carmona, I. Zimmermann, E. Mosconi, X. Lee, D. Martineau, S. Narbey, F. Oswald, F. De Angelis, M. Graetzel, M. K. Nazeeruddin, *Nat. Commun.* **2017**, *8*, 15684.

[11] E. Mosconi, D. Meggiolaro, H. J. Snaith, S. D. Stranks, F. De Angelis, *Energy Environ. Sci.* **2016**, *9*, 3180.

[12] H.-H. Fang, F. Wang, S. Adjokatse, N. Zhao, M. A. Loi, *Adv. Funct. Mater.* **2016**, *26*, 4653.

[13] S. Chen, X. Wen, S. Huang, F. Huang, Y.-B. Cheng, M. Green, A. Ho-Baillie, *Sol. RRL* **2017**, *1*, 1600001.

[14] Y. Tian, M. Peter, E. Unger, M. Abdellah, K. Zheng, T. Pullerits, A. Yartsev, V. Sundström, I. G. Scheblykin, *Phys. Chem. Chem. Phys.* **2015**, *17*, 24978.

[15] Y. Fang, Q. Dong, Y. Shao, Y. Yuan, J. Huang, *Nat. Photonics* **2015**, *9*, 679.

[16] D. W. deQuilettes, W. Zhang, V. M. Burlakov, D. J. Graham, T. Leijtens, A. Osherov, V. Bulović, H. J. Snaith, D. S. Ginger, S. D. Stranks, *Nat. Commun.* **2016**, *7*, 11683.

[17] H. Yuan, E. Debroye, K. Janssen, H. Naiki, C. Steuwe, G. Lu, M. Moris, E. Orgiu, H. Uji-i, F. De Schryver, P. Samorì, J. Hofkens, M. Roeffaers, *J. Phys. Chem. Lett.* **2016**, *7*, 561.

[18] A. Merdasa, M. Bag, Y. Tian, E. Källman, A. Dobrovolsky, I. G. Scheblykin, *J. Phys. Chem. C* **2016**, *120*, 10711.

[19] J.-C. Blancon, H. Tsai, W. Nie, C. C. Stoumpos, L. Pedesseau, C. Katan, M. Kepenekian, C. M. M. Soe, K. Appavoo, M. Y. Sfeir, S. Tretiak, P. M. Ajayan, M. G. Kanatzidis, J. Even, J. J. Crochet, A. D. Mohite, *Science* **2017**, *355*, 1288.

[20] N. H. Nickel, F. Lang, V. V. Brus, O. Shargaieva, J. Rappich, *Adv. Electron. Mater.* **2017**, *3*, 1700158.

[21] Z. Fan, H. Xiao, Y. Wang, Z. Zhao, Z. Lin, H.-C. Cheng, S.-J. Lee, G. Wang, Z. Feng, W. A. Goddard, Y. Huang, X. Duan, *Joule* **2017**, *1*, 548.

[22] T. Leijtens, G. E. Eperon, S. Pathak, A. Abate, M. M. Lee, H. J. Snaith, *Nat. Commun.* **2013**, *4*, 2885.

[23] T. A. Berhe, W.-N. Su, C.-H. Chen, C.-J. Pan, J.-H. Cheng, H.-M. Chen, M.-C. Tsai, L.-Y. Chen, A. A. Dubale, B.-J. Hwang, *Energy Environ. Sci.* **2016**, *9*, 323.

[24] M. Era, S. Morimoto, T. Tsutsui, S. Saito, *Appl. Phys. Lett.* **1994**, *65*, 676.

[25] G. Lanty, K. Jemli, Y. Wei, J. Leymarie, J. Even, J.-S. Lauret, E. Deleporte, *J. Phys. Chem. Lett.* **2014**, *5*, 3958.

[26] L. Pedesseau, D. Sapori, B. Traore, R. Robles, H.-H. Fang, M. A. Loi, H. Tsai, W. Nie, J.-C. Blancon, A. Neukirch, S. Tretiak, A. D. Mohite, C. Katan, J. Even, M. Kepenekian, *ACS Nano* **2016**, *10*, 9776.

[27] D. Ma, Y. Fu, L. Dang, J. Zhai, I. A. Guzei, S. Jin, *Nano Res.* **2017**, *10*, 2117.

[28] C. M. M. Soe, C. C. Stoumpos, M. Kepenekian, B. Traoré, H. Tsai, W. Nie, B. Wang, C. Katan, R. Seshadri, A. D. Mohite, J. Even, T. J. Marks, M. G. Kanatzidis, *J. Am. Chem. Soc.* **2017**, *139*, 16297.

[29] D. Sapori, M. Kepenekian, L. Pedesseau, C. Katan, J. Even, *Nanoscale* **2016**, *8*, 6369.

[30] J. Even, L. Pedesseau, C. Katan, *ChemPhysChem* **2014**, *15*, 3733.

[31] T. Kondo, T. Azuma, T. Yuasa, R. Ito, *Solid State Commun.* **1998**, *105*, 253.

[32] Y. Yamamoto, G. Oohata, K. Mizoguchi, H. Ichida, Y. Kanematsu, *Phys. Status Solidi* **2012**, *9*, 2501.

[33] K. Abdel-Baki, F. Boitier, H. Diab, G. Lanty, K. Jemli, F. Lédée, D. Garrot, E. Deleporte, J. S. Lauret, *J. Appl. Phys.* **2016**, *119*, 64301.

[34] M. E. Kamminga, H. H. Fang, M. R. Filip, F. Giustino, J. Baas, G. R. Blake, M. A. Loi, T. T. M. Palstra, *Chem. Mater.* **2016**, *28*, 4554.

[35] S. Pathak, N. Sakai, F. Wisnivesky Rocca Rivarola, S. D. Stranks, J. Liu, G. Eperon, C. Ducati, K. Wojciechowski, J. T. Griffiths, A. A. Haghighirad, A. Pellaroque, R. H. Friend, H. J. Snaith, *Chem. Mater.* **2015**, *27*, 8066.

[36] M. Yuan, L. N. Quan, R. Comin, G. Walters, R. Sabatini, O. Voznyy, S. Hoogland, Y. Zhao, E. M. Beauregard, P. Kanjanaboos, Z. Lu, D. H. Kim, E. H. Sargent, *Nat. Nanotechnol.* **2016**, *11*, 1.

[37] N. Wang, L. Cheng, R. Ge, S. Zhang, Y. Miao, W. Zou, C. Yi, Y. Sun, Y. Cao, R. Yang, Y. Wei, Q. Guo, Y. Ke, M. Yu, Y. Jin, Y. Liu, Q. Ding, D. Di, L. Yang, G. Xing, H. Tian, C. Jin, F. Gao, R. H. Friend, J. Wang, W. Huang, *Nat. Photonics* **2016**, *10*, 699.

[38] M. Wei, W. Sun, Y. Liu, Z. Liu, L. Xiao, Z. Bian, Z. Chen, *Phys. Status Solidi* **2016**, *213*, 2727.

[39] Y. Chen, Y. Sun, J. Peng, J. Tang, K. Zheng, Z. Liang, *Adv. Mater.* **2017**, *30*, 1703487.

[40] S. Adjokatse, H.-H. Fang, M. A. Loi, *Mater. Today* **2017**, *20*, 413.

[41] Y. Liu, H. Xiao, W. A. Goddard, *Nano Lett.* **2016**, *16*, 3335.

[42] F. Lédée, G. Trippé-Allard, H. Diab, P. Audebert, D. Garrot, J.-S. Lauret, E. Deleporte, *CrystEngComm* **2017**, *19*, 2598.

[43] G. Z. Magda, J. Pet, G. Dobrik, C. Hwang, L. P. Biró, L. Tapasztó, *Sci. Rep.* **2015**, *5*, 14714.

[44] H. Li, J. Wu, X. Huang, G. Lu, J. Yang, X. Lu, Q. Xiong, H. Zhang, *ACS Nano* **2013**, *7*, 10344.

[45] W. Liu, J. Xing, J. Zhao, X. Wen, K. Wang, P. Lu, Q. Xiong, *Adv. Opt. Mater.* **2017**, *5*, 1601045.

[46] J. Zhang, T. Song, Z. Zhang, K. Ding, F. Huang, B. Sun, *J. Mater. Chem. C* **2015**, *3*, 4402.

[47] Y. Han, S. Meyer, Y. Dkhissi, K. Weber, J. M. Pringle, U. Bach, L. Spiccia, Y.-B. Cheng, *J. Mater. Chem. A* **2015**, *3*, 8139.

[48] C. Wu, K. Chen, D. Y. Guo, S. L. Wang, P. G. Li, *RSC Adv.* **2018**, *8*, 2900.

[49] G. Batignani, G. Fumero, A. R. S. Kandada, G. Cerullo, M. Gandini, C. Ferrante, A. Petrozza, T. Scopigno, *arXiv:1705.08687* **2017**.

[50] X. Wu, L. Z. Tan, X. Shen, T. Hu, K. Miyata, M. T. Trinh, R. Li, R. Coffee, S. Liu, D. A. Egger, I. Makasyuk, Q. Zheng, A. Fry, J. S. Robinson, M. D. Smith, B. Guzelturk, H. I. Karunadasa,

1800305 (10 of 11)

**ADVANCED
SCIENCE NEWS**

www.advancedsciencenews.com

**ADVANCED
FUNCTIONAL
MATERIALS**

www.afm-journal.de

X. Wang, X. Zhu, L. Kronik, A. M. Rappe, A. M. Lindenberg, *Sci. Adv.* **2017**, *3*, e1602388.

[51] J. Calabrese, N. L. Jones, R. L. Harlow, N. Herron, D. L. Thorn, Y. Wang, *J. Am. Chem. Soc.* **1991**, *113*, 2328.

[52] Z. Wang, Q. Lin, F. P. Chmiel, N. Sakai, L. M. Herz, H. J. Snaith, *Nat. Energy* **2017**, *2*, 17135.

[53] A. V. Stier, N. P. Wilson, G. Clark, X. Xu, S. A. Crooker, *Nano Lett.* **2016**, *16*, 7054.

[54] K. S. Novoselov, A. K. Geim, S. V Morozov, D. Jiang, Y. Zhang, S. V. Dubonos, I. V. Grigorieva, A. A. Firsov, *Science* **2004**, *306*, 666.

[55] G. M. Sheldrick, *IUCr, Acta Cryst.* **2015**, *C71*, 3.

1800305 (11 of 11)